One-Dimensional Stacking of Bifunctional Dithia- and Diselenadiazolyl Radicals

Andrews, M.P.; Douglass, D.C.; Fleming, R.M.; Glarum, S.H.; Haddon, R.C.; Marsh, P.; Oakley, R.T.; Palstra, Thomas; Schneemeyer, L.F.; Trucks, G.W.

Published in:
Journal of the American Chemical Society

DOI:
10.1021/ja00009a051

Publication date:
1991

One-Dimensional Stacking of Bifunctional Dithia- and Diselenadiazolyl Radicals: Preparation and Structural and Electronic Properties of 1,3-[$(E_2N_2C)C_6H_4(CN_2E_2)$] (E = S, Se)

M. P. Andrews,[1a] A. W. Cordes,*[,1b] D. C. Douglass,[1a] R. M. Fleming,[1a] S. H. Glarum,[1a] R. C. Haddon,*[,1a] P. Marsh,[1a] R. T. Oakley,*[,1c] T. T. M. Palstra,[1a] L. F. Schneemeyer,[1a] G. W. Trucks,[1a] R. Tycko,[1a] J. V. Waszczak,[1a] K. M. Young,[1c] and N. M. Zimmerman[1a]

Contribution from AT&T Bell Laboratories, Murray Hill, New Jersey 07974, Department of Chemistry and Biochemistry, University of Arkansas, Fayetteville, Arkansas 72701, and Guelph Waterloo Centre for Graduate Work in Chemistry, Guelph Campus, Department of Chemistry and Biochemistry, University of Guelph, Guelph, Ontario N1G 2W1, Canada.
Received October 1, 1990

Abstract: The preparation and solid-state characterization of the 1,3-phenylene-bridged bis(dithiadiazolyl) and bis(diselenadiazolyl) diradicals 1,3-[$(E_2N_2C)C_6H_4(CN_2E_2)$] (E = S, Se) are reported. The isomorphous crystals of 1,3-[$(E_2N_2C)C_6H_4(CN_2E_2)$] so obtained are tetragonal, space group $I4_1/a$. Stacks of diradical molecules, linked vertically in a zigzag fashion through alternate ends by long E---E contacts (mean 3.140/3.284 Å for E = S/Se), are arranged in pinwheellike clusters about the 4_1 and $\bar{4}$ axes, producing complex patterns of interstack E---E contacts. Both compounds show the presence of spin defects in the lattice, and there is a very large enhancement in the paramagnetism of the sulfur compound at high temperatures. The selenium compound is a semiconductor, with a room temperature conductivity of 2×10^{-4} S cm^{-1}. Solid-state NMR experiments find enhanced relaxation times, which have their origin in the presence of a mobile paramagnetic defect. Extended Hückel band structure calculations show the materials to be semiconductors, with band gaps of about 1.0/0.8 eV for E = S/Se. Although the compounds adopt a columnar structure, the calculations indicate significant interactions between the stacks and the materials exhibit well-developed three dimensionality. The enhanced paramagnetism in the sulfur compound is attributed to the presence of thermally generated phase kinks in the lattice, whereas the selenium compound is classified as an intrinsic semiconductor.

Introduction

We are interested in the design of low-dimensional molecular materials constructed from neutral as opposed to ionic radicals. While the latter materials, which include simple charge transfer salts, e.g., TTF TCNQ,[2] and also the Bechgaard-type salts based on donors such as TMTSF and BEDT-TTF,[3] have afforded much insight into the general strategy of molecular metal design, the former hold several potential advantages.[4] A variety of systems based on the originally proposed phenalenyl "building block" have been investigated,[5] but the comparison of theory and experiment has been hindered by the absence of structural data. Recent advances in the design of thermodynamically stable hetrocyclic thiazyl and selenazyl radicals,[6] however, have prompted the exploration of such systems as molecular building blocks.[7] Within this context the 1,2,3,5-dithiadiazolyl and 1,2,3,5-diselenadiazolyl radicals **1** (E = S, Se) are attractive candidates. Synthetic strategies to such species are well-developed, and the cumulative evidence of ESR, photoelectron and theoretical studies has provided a clear picture of their electronic structure;[8] the unpaired electron in these derivatives is confined to the a_2 distribution **2**. Consistently, hyperfine coupling constants to nitrogen and ionization potentials are relatively invariant to substituent effects.

Our initial approach to the construction of molecular conductors from such radicals has been to design systems in which two radical centers are incorporated into a single molecule. Recently we described the preparation and solid-state characterization of the 1,4-phenylene bridged 1,2,3,5-dithiadiazolyl and 1,2,3,5-diselenadiazolyl diradicals **3** (E = S, Se).[9] These materials are iso-

(1) AT&T Bell Laboratories. (b) University of Arkansas. (c) University of Guelph.

(2) See, for example: (a) Garito, A. F.; Heeger, A. J. *Acc. Chem. Res.* **1974**, *7*, 232. (b) Torrance, J. B. *Acc. Chem. Res.* **1979**, *12*, 79. (c) Perlstein, J. H. *Angew. Chem., Int. Ed.* **1977**, *16*, 519.

(3) (a) Wudl, F. *Acc. Chem. Res.* **1984**, *17*, 227. (b) Williams, J. M.; Beno, M. A.; Wang, H. H.; Leung, P. C. W.; Emge, T. J.; Geiser, U.; Carlson, K. D. *Acc. Chem. Res.* **1985**, *18*, 261. (c) Williams, J. M.; Wang, H. H.; Emge, T. J.; Gieser, U.; Beno, M. A.; Leung, P. C. W.; Carlson, K. D.; Thorn, R. J.; Schultz, A. J.; Whangbo, M.-H. *Prog. Inorg. Chem.* **1987**, *35*, 51. (d) Inokuchi, H. *Angew. Chem., Int. Ed.* **1988**, *27*, 1747.

(4) (a) Haddon, R. C. *Nature (London)* **1975**, *256*, 394. (b) Haddon, R. C. *Aust. J. Chem.* **1975**, *28*, 2343.

(5) (a) Haddon, R. C.; Wudl, F.; Kaplan, M. L.; Marshall, J. H.; Cais, R. E.; Bramwell, F. B. *J. Am. Chem. Soc.* **1978**, *100*, 7629. (b) Kaplan, M. L.; Haddon, R. C.; Hirani, A. M.; Schilling, F. C.; Marshall, J. H. *J. Org. Chem.* **1981**, *46*, 675. (c) Haddon, R. C.; Chichester, S. V., Stein, S. M.; Marshall, J. H.; Mujsce, A. M. *J. Org. Chem.* **1987**, *52*, 711. (d) Canadell, E.; Shaik, S. S. *Inorg. Chem.* **1987**, *26*, 3797. (e) Nakasuji, K.; Yamaguchi, M.; Murata, I.; Yamaguchi, K.; Fueno, T.; Ohya-Nishiguchi, H.; Sugano, T.; Kinoshito, M. *J. Am. Chem. Soc.* **1989**, *111*, 9265.

(6) (a) Oakley, R. T. *Prog. Inorg. Chem.* **1988**, *36*, 299. (b) Preston, K. F.; Sutcliffe, L. H. *Magn. Reson. Chem.* **1990**, *28*, 189.

(7) (a) Wolmershäuser, G.; Schnauber, M.; Wilhelm, T. *J. Chem. Soc., Chem. Commun.* **1984**, 573. (b) Wolmershäuser, G.; Schnauber, M.; Wilhelm, T.; Sutcliffe, L. H. *Synth. Met.* **1986**, *14*, 239. (c) Dormann, E.; Nowak, M. J.; Williams, K. A.; Angus, R. O., Jr.; Wudl, F. *J. Am. Chem. Soc.* **1987**, *109*, 2594. (d) Wolmershäuser, G.; Wortmann, G.; Schnauber, M. *J. Chem. Res., Synop.* **1988**, 358. (e) Wolmershäuser, G.; Johann, R. *Angew. Chem., Int. Ed.* **1989**, *28*, 920. (f) Hayes, P. J.; Oakley, R. T.; Cordes, A. W.; Pennington, W. T. *J. Am. Chem. Soc.* **1985**, *107*, 1346. (g) Boerē, R. T.; Cordes, A. W.; Hayes, P. J.; Oakley, R. T.; Reed, R. W. *Inorg. Chem.* **1986**, *25*, 2445. (h) Oakley, R. T.; Reed, R. W.; Cordes, A. W.; Craig, S. L.; Graham, J. B. **1987**, *109*, 7745. (i) Boerē, R. T.; French, C. L.; Oakley, R. T.; Cordes, A. W.; Privett, J. A. J.; Craig, S. L.; Graham, J. B. *J. Am. Chem. Soc.* **1985**, *107*, 7710. (j) Awere, E. G.; Burford, N.; Haddon, R. C.; Parsons, S.; Passmore, J.; Waszczak, J. V.; White, P. S. *Inorg. Chem.* **1990**, *29*, 4821. (k) Wolmershäuser, G.; Kraft, G. *Chem. Ber.* **1990**, *123*, 881.

(8) Vegas, A.; Perēz-Salazar, A.; Banister, A. J.; Hey, R. G. *J. Chem. Soc., Dalton Trans.* **1980**, 1812. (b) Hofs, H.-U.; Bats, J. W.; Gleiter, R.; Hartmann, G.; Mews, R.; Eckert-Maksič, M.; Oberhammer, H.; Sheldrick, G. M. *Chem. Ber.* **1985**, *118*, 3781. (c) Fairhurst, S. A.; Johnson, K. M.; Sutcliffe, L. H.; Preston, K. F.; Banister, A. J.; Hauptmann, Z. V.; Passmore, J. *J. Chem. Soc., Dalton Trans.* **1986**, 1465. (d) Boerē, R. T.; Oakley, R. T.; Reed, R. W.; Westwood, N. P. C. *J. Am. Chem. Soc.* **1989**, *111*, 1180. (e) Banister, A. J.; Hansford, M. I.; Hauptmann, Z. V.; Wait, S. T.; Clegg, W. *J. Chem. Soc., Dalton Trans.* **1989**, 1705. (f) Cordes, A. W.; Goddard, J. D.; Oakley, R. T.; Westwood, N. P. C. *J. Am. Chem. Soc.* **1989**, *111*, 6147.

(9) (a) Cordes, A. W.; Haddon, R. C.; Oakley, R. T.; Schneemeyer, L. F.; Waszczak, J. A.; Young, K. M.; Zimmerman, N. M. *J. Am. Chem. Soc.* **1991**, *113*, 582. (b) Del Bel Belluz, P.; Cordes, A. W.; Kristof, E. M.; Kristof, P. V.; Liblong, S. W.; Oakley, R. T. *J. Am. Chem. Soc.* **1989**, *111*, 9276.

0002-7863/91/1513-3559$02.50/0

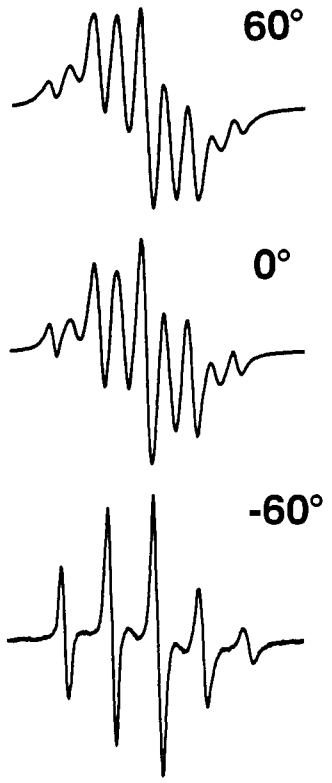

Figure 1. ESR spectrum of **4** (E = S) in $CHCl_3$.

morphous and pack as interleaved arrays of discrete diradical dimers. The sulfur compound is an insulator but the selenium derivative exhibits a room temperature pressed pellet conductivity of about 10^{-2} S cm^{-1}. Extended Hückel band structure calculations reveal the structures to have a significant degree of three dimensionality.

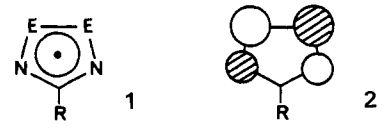

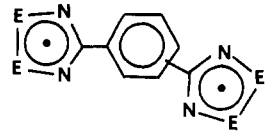

3 (1,4)
4 (1,3)

As a continuation of this work we have prepared and characterized the isomeric 1,3-phenylene bridged diradicals **4** (E = S, Se). Herein we report the crystal and molecular structures of these compounds and also provide details of their magnetic and conductivity properties. The results are discussed in the light of extended Hückel band structure calculations.

Results and Discussion

Preparation of 1,3-[$(E_2N_2C)C_6H_4(CN_2E_2)$] (E = S, Se). The dichloride salts 1,3-[$(E_2N_2C)C_6H_4(CN_2E_2)$]Cl_2 (E = S, Se) were prepared as previously described for the corresponding 1,4-derivatives. The necessary starting material, 1,3-phenylenebis-[tris(trimethylsilyl)amidine], can be prepared by treatment of 1,3-dicyanobenzene with lithium bis(trimethylsilyl)amide, followed by transmetalation of the intermediate *N*-lithio derivative with trimethylsilyl chloride. Reduction of the crude dichlorides with triphenylantimony in acetonitrile affords the diradicals **4** as black, virtually insoluble powders. As before, the products were purified by vacuum sublimation at 140 °C/10^{-2} Torr (E = S) and 180 °C/10^{-6} Torr (E = Se).

Solution-State ESR Measurements. ESR parameters have been reported for a wide range of monofunctional dithiadiazolyls **1** (E = S).[8b-d,f] The ESR spectrum of **1** (E = Se, R = Ph) has also been reported; its *g* value (2.0394) is predictably larger,[9b] approaching those found for $[SN_2Se_2]^{\bullet+}$ and $[SeN_2Se_2]^{\bullet+}$.[10] As in the case of the 1,4-diradicals **3**, ESR data for **4** is limited to E = S; for E = Se the material is sufficiently insoluble to reduce signal intensity below the detection limit. The ESR signal of **4** (E = S), recorded on a saturated solution in chloroform, has a *g* value of 2.011. As illustrated in Figure 1, the spectrum shows a temperature dependence similar to although more extensive than that seen for **3** (E = S). The observed changes are characteristic of very weak intramolecular[11] exchange coupling (J_{ex}) between two radical centers.[12] At −60 °C the spectrum resembles that expected for noninteracting radical centers, i.e., a simple five-line pattern with a_N = 0.51 mT. Above this temperature the spectrum begins to reveal the influence of exchange coupling between the two radical centers; at 60 °C the spectrum approaches the fast exchange limit in which $J_{ex} > a_N$.

Table I. Summary of Bond Lengths (Å) and Angles (deg) and Intermolecular Contacts (Å) in **4** (E = S, Se)

	E = S		E = Se	
	av	range	av	range
d(E-E)	2.084	2.078–2.090	2.335	2.323–2.352
d(E-N)	1.627	1.616–1.638	1.78	1.72–1.83
d(N-C)	1.340	1.330–1.348	1.34	1.30–1.39
E-E-N	94.6	94.0–94.9	91	89–92
E-N-C	114.3	113.8–114.8	115	110–120
N-C-N	122	121.9–122.5	128	121–135
	d_1	3.104		3.181
	d_2	3.179		3.368
	d_3	3.139		3.311
	d_4	3.136		3.277
	d_5	4.004		4.086
	d_6	3.914		3.875
	d_7	3.960		4.007
	d_8	3.984		4.090
	d_9	3.448		3.456
	d_{10}	3.711		3.714
	d_{11}	3.509		3.530
	d_{12}	3.691		3.662
	d_{13}	3.280		3.891
	d_{14}	3.817		4.613
	d_{15}	3.959		3.486
	d_{16}	4.509		3.628

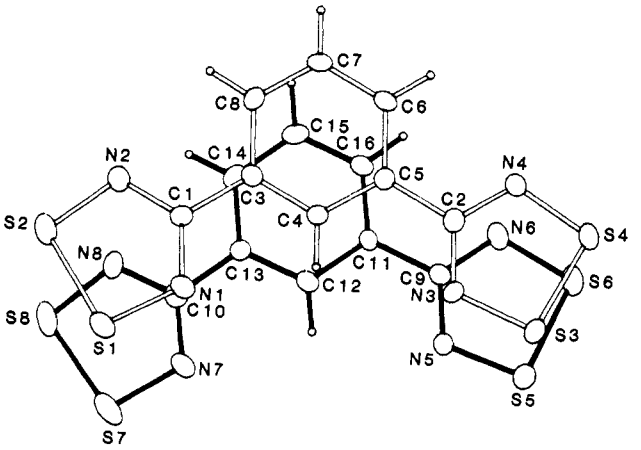

Figure 2. Atom numbering scheme used for both structures. The view shown (for E = S) is normal to the C3–C8 plane.

(10) (a) Awere, E. G.; Passmore, J.; Preston, K. F.; Sutcliffe, L. H. *Can. J. Chem.* **1988**, *66*, 1776. (b) Awere, E. G.; Passmore, J.; White, P. S.; Klapötke, T. *J. Chem. Soc., Chem. Commun.* **1989**, 1415.

(11) The low solubility of the diradicals precludes any possibility of intermolecular exchange interactions.

(12) (a) Glarum, S. H.; Marshall, J. H. *J. Chem. Phys.* **1967**, *47*, 1374. (b) Briere, P.; Dupeyre, R.-M.; Lemaire, H.; Morat, C.; Rassat, A.; Rey, P. *Bull. Chim. Soc. Fr.* **1965**, 3290. (c) Reitz, D. C.; Weissman, S. I. *J. Chem. Phys.* **1960**, *33*, 700. (d) Eaton, G. R.; Eaton, S. S. *Acc. Chem. Res.* **1988**, *21*, 107.

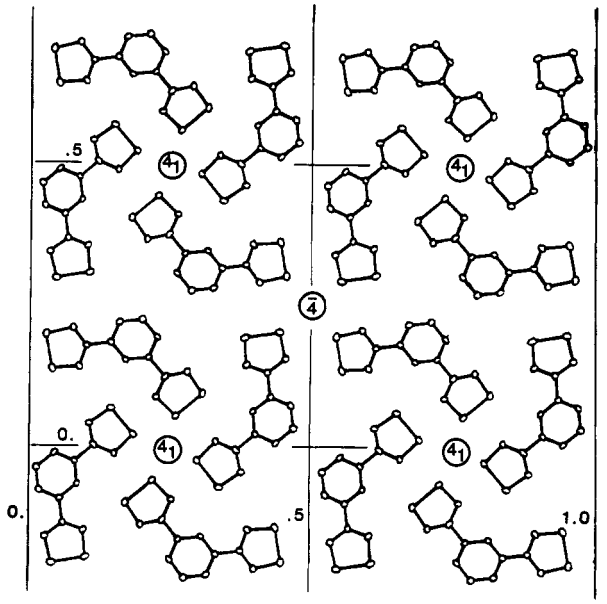

Figure 3. *xy* projection (*x* horizontal) of the cell packing. The 4_1 axes are perpendicular to this plane at the locations noted; the $\bar{4}$ points shown are at elevations of $z = 0.375$ and 0.875.

Crystal and Molecular Structures. The two diradicals **4** (E = S, Se) have isomorphous structures; the crystals are tetragonal, space group $I4_1/a$. A summary of pertinent intramolecular and intermolecular bond length and angle formation is provided in Table I. There are two crystallographically independent diradical units in the unit cell. An ORTEP drawing of a single asymmetric unit for E = S is shown in Figure 2. The mean internal structural parameters of the diradicals are similar to those seen in **3**[9] and indeed in related monofunctional radicals. The S–S and Se–Se bonds are slightly longer than in cationic structures, as are, to a lesser degree, the S–N and Se–N distances. Taken collectively the differences between the two oxidation states can be interpreted, in simple MO terms, in terms of the occupation (upon reduction) of the antibonding a_2 orbital **2**.

Within the unit cell of **4** (E = S, Se) (Figure 3) there are four pinwheellike clusters of vertically stacked arrays of diradical units parallel to the *c* axis. Each of the vertical stacks consists of molecular "plates" slightly offset from the ideal regular spacing sequence, i.e., the system has suffered a Peierls distortion. The plates, however, do not couple into discrete dimers, as in the case of the corresponding 1,4-diradical structures. Instead there is a subtle rocking of opposite ends of each molecule so as to produce a zigzag arrangement of short (mean of $d_1 - d_4 = 3.140/3.284$ Å for E = S/Se) and long (mean of $d_5 - d_8 = 3.966/4.014$ Å for E = S/Se) E---E contacts (see Figure 4 and Table I). This rocking motion of the plates does not significantly perturb the phenyl groups, for which the long and short centroid-to-centroid distances are 3.575/3.543 Å and 3.687/3.596 Å (E = S/Se). The planes of the two phenyl rings are, moreover, parallel to within 3.3/1.7° (E = S/Se).

The lattice symmetry affords two symmetrically distinct groups of intercolumnar radical–radical contacts. The two groups are distributed around, and defined by, the 4_1 axes (for example, at $x = 0.75$, $y = 0$) and the $\bar{4}$ points (for example, at $x = 0.50$, $y = 0.25$, $z = 0.375$) (see Figure 3). The origins of the subtle differences in the clustering of the radical dimers about these symmetry elements can be understood with reference to Scheme I, which illustrates the effects of different Peierls distortions of the idealized array A composed of the nearest chalcogen–chalcogen contacts distributed consistently with the presence of both 4_1 and $\bar{4}$ symmetry elements. All three structures B, C, and D share a common feature, namely, bond alternation (and unit cell doubling) in the *c* direction. The bond alternation waves along the four columnar components are, however, characterized by different phase factors. In case B one set of 4_1-related atoms moves upward

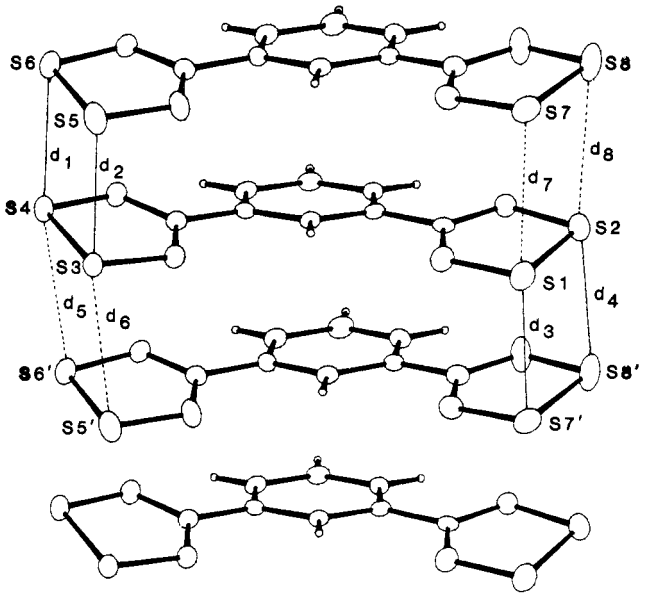

Figure 4. Zigzag coupling along vertical stacks of diradicals.

Scheme I

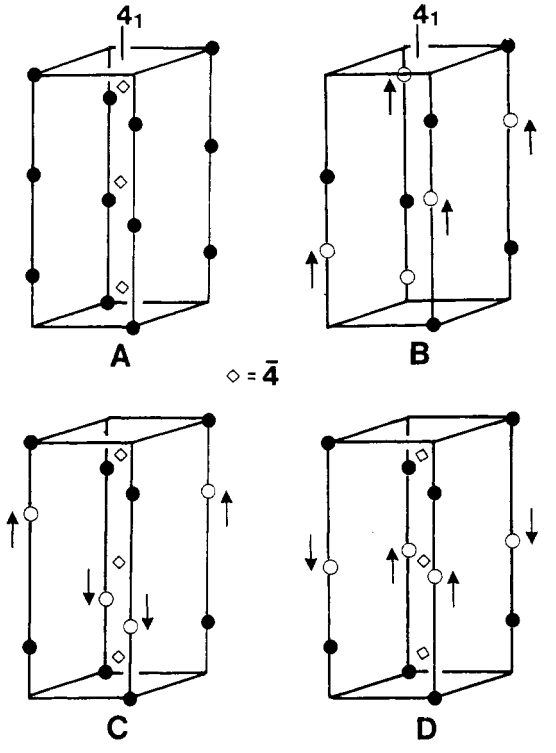

in unison, generating two distinct spiral arrays of close intercolumnar contacts about the 4_1 axis; this arrangement is common to both the sulfur- and selenium-based compounds and is shown (for E = S) in Figure 5. The short E---E contacts d_{10}–d_{12} are listed in Table I.

In structures C and D alternate sets of atoms clustered about $\bar{4}$ points are elongated (in C) or compressed (in D) approximately along *c* in a manner that conserves the $\bar{4}$ symmetry. Depending on whether the motion is expansive or compressive the short intercolumnar contacts generated will be either between symmetry unrelated (in C) or related (in D) positions. In the sulfur-based structure the assembly of $\bar{4}$ points is of type C, with short S2---S8′ contacts (d_{13} and d_{14}), while in the selenium derivative the $\bar{4}$ points generate a structure of type D, with close Se2---Se2 (d_{15}) and Se8---Se8 (d_{16}) approaches. The actual atomic arrangements about these points in both structures is illustrated in Figure 6 (A and B).

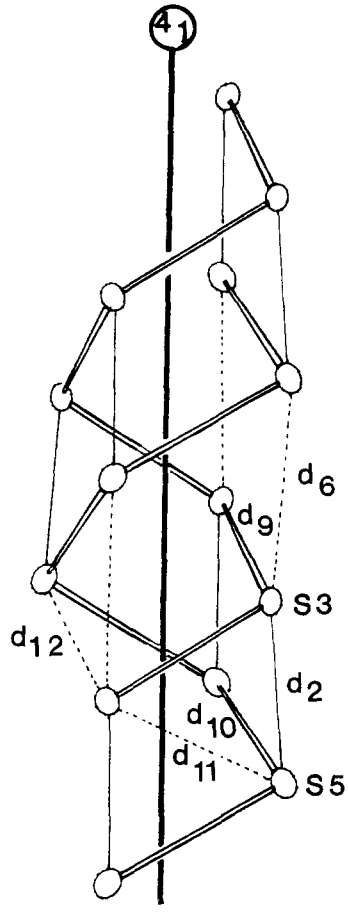

Figure 5. S---S (Se---Se) contacts around the 4_1 screw axis. The hollow bonds connect like atoms related by the screw axis, with spacings d_9 for S3 (Se3) and d_{10} for S5 (Se5).

Solid-State Magnetic Measurements. The measured magnetic susceptibilities of **4** (E = S, Se) as a function of temperature are shown in Figures 7 and 8. The low-temperature susceptibilities of both compounds show Curie behavior, due to the presence of a small concentration of defects, which are associated with unpaired electrons. The concentration of paramagnetic defects from a Curie-Weiss fit to the data presented in the figures was found to be 0.97% (E = S) and 0.51% (E = Se) on a per molecule basis; these values are similar to those found previously for **3** (E = S).[9a] The θ values were 7 and −1 K and the measured diamagnetism amounted to −160 and −164 ppm emu mol^{-1} for E = S and Se, respectively.

ESR measurements on single crystals of the compounds produced very similar results, although there is some variation between crystals in the concentration of paramagnetic defects. In the case of the samples whose ESR spectra (E = S) appear in Figures 9 and 10 the concentration of spins was found to be 0.50% and 0.82%, respectively. The high-temperature behavior of the susceptibilities is most unusual, particularly in the case of the sulfur compound. Both compounds show an increased paramagnetic contribution to the susceptibility as the temperature is raised and ultimately undergo decomposition. By assuming that the paramagnetism may be described by a Curie relationship, the mole fraction of spins is plotted as a function of temperature in Figure 11, as determined from the bulk magnetic susceptibility and single-crystal ESR studies. The bulk magnetic susceptibility and single-crystal ESR results show good agreement between room temperature and 200 °C. Although not obvious from the figure, the concentration of spins, as determined from both the magnetic susceptibility and ESR measurements, initially decreases above room temperature for E = S but not for the selenium compound, which increases monotonically. In the case of the sample shown in Figure 10, the room temperature fraction of spins of 0.82% fell to 0.52% at 50 °C, before starting a monotonic increase. This

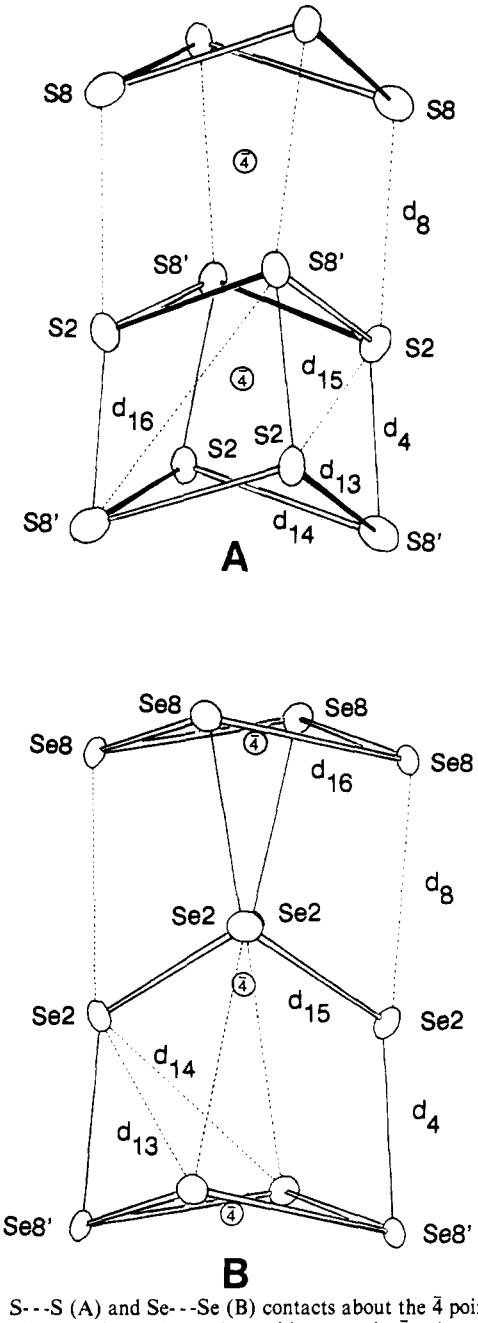

Figure 6. S---S (A) and Se---Se (B) contacts about the $\bar{4}$ points. The two S-containing radical units are located between the $\bar{4}$ points such that the two shortest contacts are S2---S8′ (the solid and hollow bonds). The Se units are closer to the $\bar{4}$ points such that the shortest contacts are Se2---Se2 and Se8---Se8 (hollow bonds).

may suggest that initially some of the defects in the lattice of the sulfur compound are annealed above room temperature, before thermal energy begins to break the radical–radical bonds and increase the concentration of paramagnetic defects. It may also be seen in Figure 11 that the ESR line width at first broadens, which would suggest that just above room temperature the spins initially become more localized, before undergoing an increase in motion around 360 K as the concentration of defects begins a substantial increase and the ESR line width narrows again. At about 410 K the line width broadens once more, presumably as a result of dipolar interactions between pairs of electrons as the concentrations of spins becomes significant. The break in the rise in spin concentration of the sulfur compound as shown in Figures 7 and 11 at about 450 K cannot be easily explained; careful inspection of the data from the selenium compound suggests a similar but vastly smaller feature at about 480 K.

Magnetic studies of the sulfur compound are reversible up to about 170 °C, although molecular decomposition does not appear

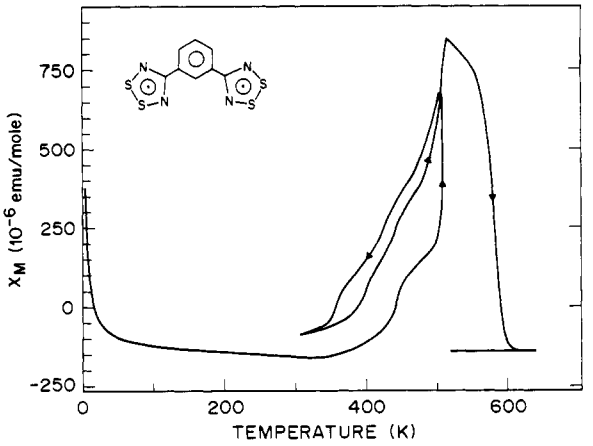

Figure 7. Magnetic susceptibility of **4** (E = S) as a function of temperature.

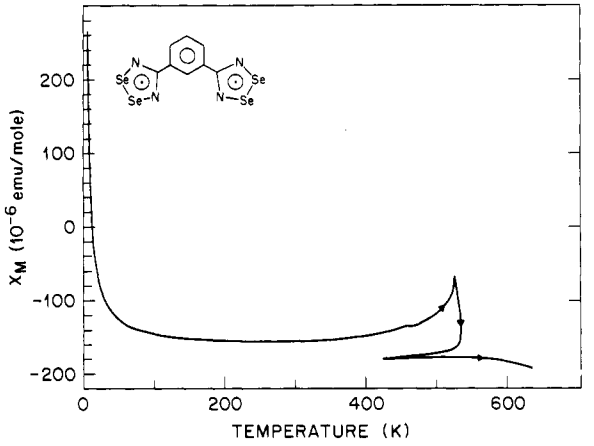

Figure 8. Magnetic susceptibility of **4** (E = Se) as a function of temperature.

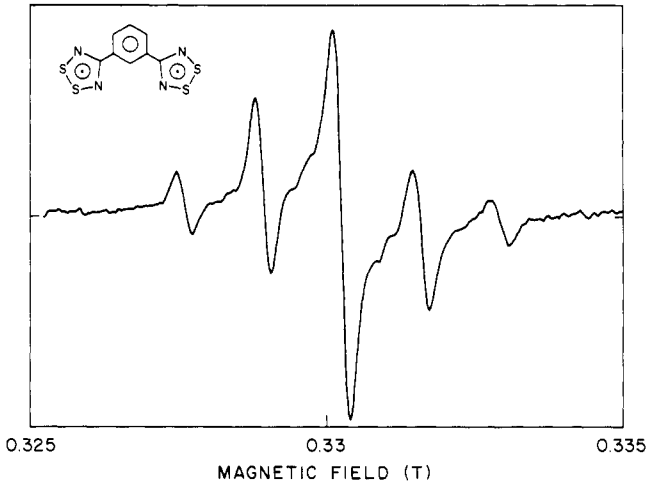

Figure 9. ESR spectrum of a single crystal of **4** (E = S) with the applied magnetic field perpendicular to the *c* axis at 4 K (see text).

to set in at an appreciable rate below about 230 °C. Between these two temperatures the dimers fragment, and some of these breaks persist as paramagnetic defects in the lattice on cooling the sample.

As noted above, there is some variability in the magnetic properties of the samples, presumably due to the vagaries of crystal growth in the sublimation process. Representative ESR single-crystal spectra with the *c* axis of the crystal perpendicular to the applied field are shown in Figures 9 and 10. The well-resolved spectrum (Figure 9) taken at 9 K shows the characteristic five-line pattern of the dithiadiazolyl ring system, and there is therefore

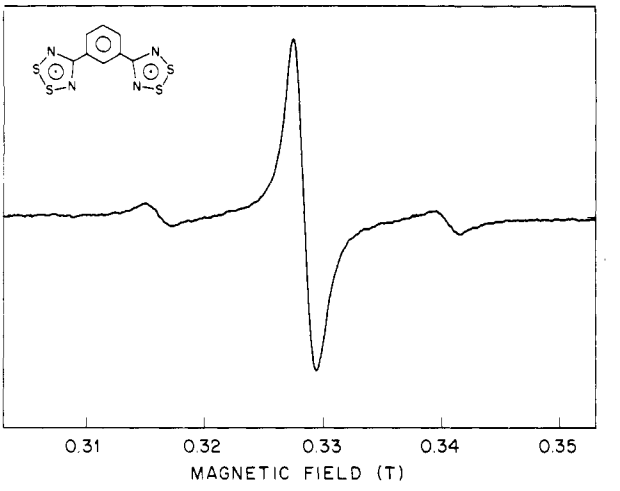

Figure 10. ESR spectrum of a single crystal of **4** (E = S) with the applied magnetic field perpendicular to the *c* axis at room temperature (see text).

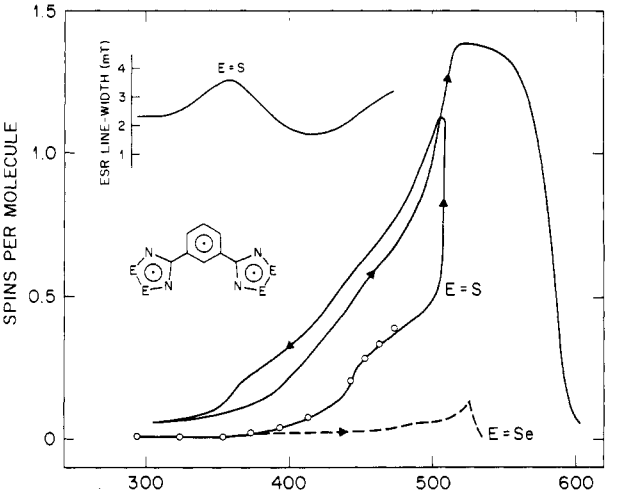

Figure 11. Spin concentration per molecule for **4** (E = S and Se) from magnetic susceptibility (- - -) and ESR (○) measurements and ESR line width for **4** (E = S) as a function of temperature.

little doubt that the paramagnetic defects are uncoupled monomers, with an electronic configuration similar to that giving rise to the solution spectra previously discussed. The spectral parameters at 9 K are g_{zz} = 2.0021 and a^{zz}_N = 1.331 mT. The nitrogen coupling constant is temperature dependent and the following values are obtained: 1.334 mT (19 K), 1.328 (54), 1.319 (105), 1.297 (200), 1.264 (250), 1.238 (300). This sample showed the expected 4-fold symmetry for the tetragonal lattice. The spectrum shown in Figure 10 is not well-resolved and contains a higher concentration of spins. Of most interest, however, are the satellites to the main peak, which are located at +11.9 and −12.4 mT relative to the center line, for a total splitting of 24.3 mT. Assuming this splitting is due to dipolar coupling between pairs of electrons leads to a separation of 4.25 Å between the interacting centers. This splitting is temperature dependent, and at a temperature of 246 K increases to 26.8 mT, which corresponds to a separation of 4.11 Å between the centers of spin. Above room temperature the satellites broaden and by the time the sample temperature has reached 100 °C they have merged with the center line. Nevertheless the satellites were essentially unchanged in position and intensity after returning the sample to room temperature after an excursion to 200 °C to obtain the data shown in Figure 11, even though the total spin concentration was enhanced by a factor of 4.4 as a result of this treatment.

Solid-State NMR Measurements. NMR measurements were carried out on polycrystalline samples of the sulfur and selenium compounds. At room temperature the proton spin–lattice re-

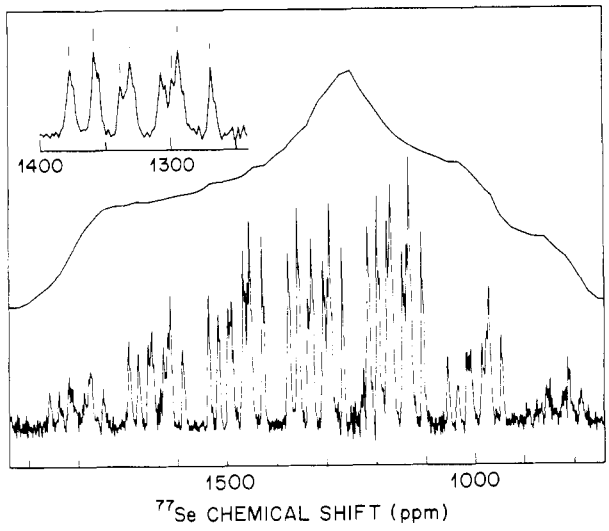

Figure 12. Magic angle spinning spectrum of **4** (E = Se) at 38.2 MHz and 295 K compared with the static sample spectrum (upper envelope). The inset shows the center-band isotropic shifts on an expanded scale.

laxation time (T_1) is 130 ms for **4**, E = S at 100 MHz, and 320 and 490 ms for E = Se at 100 and 300 MHz, respectively. These T_1 values are at least 2 orders of magnitude less than the T_1 expected for a typical rigid, diamagnetic, insulating organic solid. The field dependence of T_1 for the selenium compound is inconsistent with relaxation by conduction electrons, which would lead to a field-independent T_1. The absence of a discernible Knight shift supports this conclusion. We attribute the rapid relaxation to the presence of a mobile paramagnetic species, associated with either defect sites or thermally excited carriers.

Measurements of ^{77}Se spin–lattice relaxation in the selenium compound at 57.1 MHz reveal a strongly orientation dependent T_1, leading to a highly nonexponential decay of longitudinal magnetization, with T_1 lying principally between 10 and 100 ms at 295 K; owing to the 6.5% natural abundance of ^{77}Se, spin diffusion gives no effective averaging of this distribution in T_1 values. The relaxation mechanism is therefore assignable to an anisotropic hyperfine coupling that is substantially larger than the isotropic hyperfine component. The near equivalence of the Carr-Purcell spin–spin relaxation rate with the spin–lattice relaxation rate shows that the motion of the paramagnetic species is rapid on the Larmor time scale of 5×10^{-8} s.

The T_1 of ^{77}Se has a temperature dependence that is consistent with a thermally activated relaxation mechanism, with an activation energy of 7.2 kcal mol^{-1} from −30 to 70 °C. Magic angle spinning (MAS) and static sample ^{77}Se spectra, obtained at room temperature at 38.2 MHz, are shown in Figure 12. The proton-decoupled MAS spectrum is well-fitted by eight sets of isotropic lines and spinning sidebands, with equal total intensity associated with each set. Under MAS conditions, the eight sets of lines have the same single T_1, within experimental error, indicating that the relaxation process is spatially homogeneous and the same for all selenium positions on the T_1 time scale of milliseconds. A preliminary analysis of the spinning/sideband intensities[13] associated with one of the better resolved sets (δ_{iso} = 1383 ppm) leads to the following chemical shift tensor components: δ_{33} = 1854, δ_{22} = 1283, and δ_{11} = 995 ppm. The shifts are referenced to dimethylselenium on a δ scale,[14] using a selenous acid solution as a secondary reference with δ = 1282 ppm. It is clear from the static sample spectrum that the remaining sites have components of similar magnitudes and positions, grouped into two subsets of more closely similar tensors. An analysis of the shift tensors for the remaining sites, and the anisotropic hyperfine interaction, will be given in a more detailed presentation.

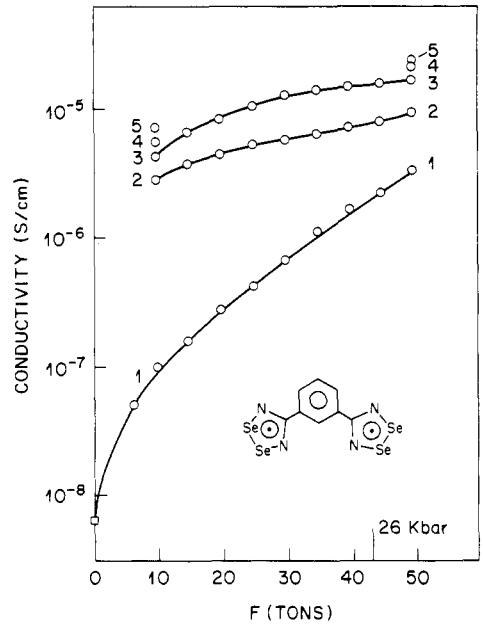

Figure 13. Room temperature conductivity of **4** (E = Se) as a function of pressure. The five plots refer to the conductivity of a single sample subjected to a series of pressure applications.

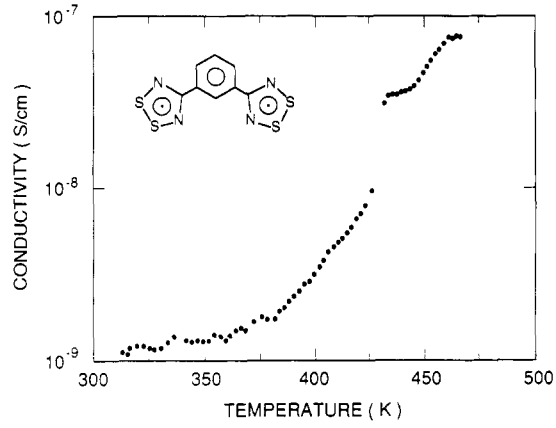

Figure 14. Single-crystal conductivity of **4** (E = S) as a function of temperature.

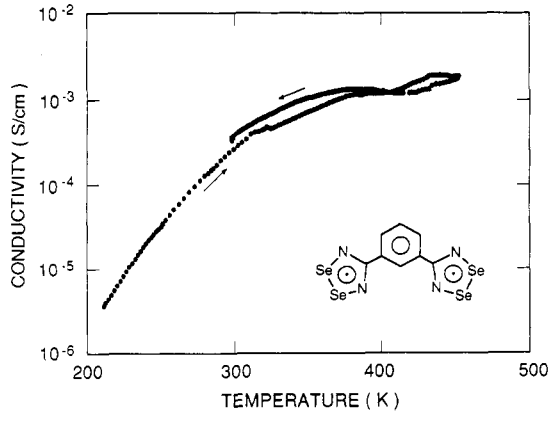

Figure 15. Single-crystal conductivity of **4** (E = Se) as a function of temperature.

Conductivity Measurements. The room temperature conductivity of the selenium compound **4** (E = Se) as a function of pressure under quasi-hydrostatic conditions is shown in Figure

(13) Herzfeld, J.; Berger, A. E. *J. Chem. Phys.* **1980**, *73*, 6021.
(14) (a) Harris, R. K.; Mann, B. E., Eds. *NMR and the Periodic Table*; Academic: New York, 1978; pp 402–406. (b) Sukhovskii, A. A.; Moskvich, Yu. N.; Lundin, A. G. *Proceedings of the XXth Congress Ampere, Tallinn, 1978*; Kunkla, E., Lippmaa, E., Saluvere, T., Eds.; Springer-Verlag: New York, 1979; p 101.

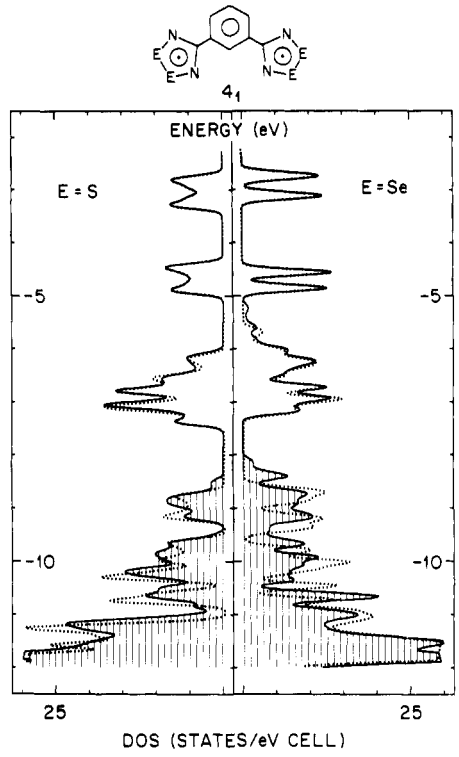

Figure 16. Calculated density of states of a 1-d stack of dimers (···) and a 1-d stack of four dimers (---) according to the crystal structure at the 4_1 axis of **4**.

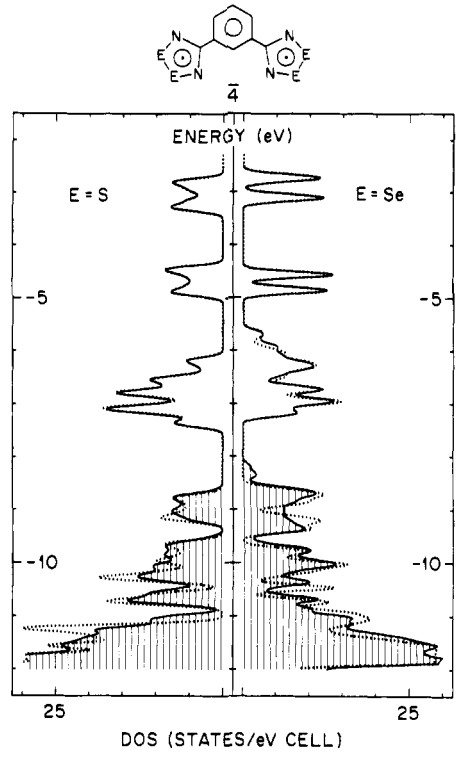

Figure 17. Calculated density of states of a 1-d stack of dimers (···) and a 1-d stack of four dimers (---) according to the crystal structure at the $\bar{4}$ axis of **4**.

13. Under the same conditions the sulfur compound (**4**, E = S) proved to be an insulator at all accessible pressures. The pressed pellet results shown in Figure 13 provide an interesting comparison with the conductivity determination of **3** (E = Se),[9a] which showed little pressure dependence. The present material is more sensitive to pressure, but this could be a reflection of the dimensionality of the two classes of compounds.

Four-probe single-crystal conductivity measurements of the compounds as a function of temperature are shown in Figures 14 and 15. It may be seen that the sulfur compound, while an insulator at room temperature, does begin to exhibit a small conductivity, which reaches a maximum of about 10^{-7} S cm^{-1} at 470 K. This corresponds to the region just above the knee in the magnetic susceptibility (Figure 7).

The conductivity of a single crystal of the selenium compound at 200 K is about 10^{-6} S cm^{-1} measured along the needle axis, and this rapidly increases as the temperature is raised to reach a value of 2×10^{-3} S cm^{-1} at 470 K. The conductivity of the selenium compound has a temperature dependence that is consistent with a thermally activated process with an activation energy of 0.55 eV (13 kcal mol^{-1}) between 200 and 300 K. If the material is treated as an intrinsic semiconductor, then at the simplest level of band theory[15] a carrier density of 5.8×10^{14} cm^{-3} (1.3×10^{-6} per molecule) may be calculated at room temperature. The mobility thus obtained is 2.2 cm^2 V^{-1} s^{-1}.

Band Structure Calculations. One-dimensional band structure calculations have been carried out on structural subunits of the experimental crystal structure by using extended Hückel theory as described previously.[9a] The three structural subunits considered are (i) a single 1-d stack of dimers, (ii) a 1-d stack of four dimers according to the pinwheel structure at the 4_1 axis, and (iii) a 1-d stack of four dimers according to the pinwheel structure at the $\bar{4}$ axis (Figures 3–6). The results are presented in Figures 16–18 in the form of density of states and dispersion curves. The dotted lines in the figures represent the results for the single stack calculations, whereas the solid curves represent the calculation

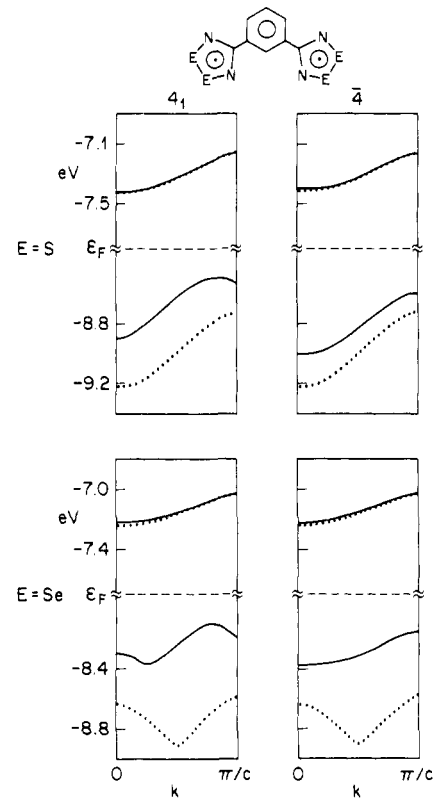

Figure 18. One-dimensional dispersion curves for the valence and conduction bands, according to the scheme given in the captions to Figures 16 and 17.

for the pinwheel-like clusters in the two symmetries found in the crystal structure.

It may be seen from the density of states curves that in all cases the calculations find the materials to be semiconductors. The transition from an isolated stack to a four-molecule cluster exerts a large effect on the band structure, particularly in the case of

(15) Ashcroft, N. W.; Mermin, N. D. *Solid State Physics*; Saunders: New York, 1976; p 575.

the selenium compound, and this is most pronounced for the 4_1 axis. These interactions serve to move states into the gap, and it is clear that in spite of the 1-d stacked structure in these compounds there is considerable three dimensionality in the electronic structure of these materials. The 1-d band gaps are calculated to be 1.16, 1.20 eV (single stack), 0.96, 0.78 eV (four molecules at the 4_1 axis), and 1.12, 0.84 eV (four molecules at the $\bar{4}$ axis), for E = S and Se, respectively. It is interesting to note that the calculations find the band gap for a single stack of molecules to be least for the sulfur compound but that the interactions within a four-molecule cluster are sufficient to reverse the situation.

The dispersion curves emphasize the importance of three dimensionality, particularly in the selenium compound and especially with respect to its effect on the valence band. In contrast with the 1,4-derivatives, **3**,[9a] it is notable that the calculations predict the 1,3-derivatives to be indirect band gap semiconductors.

Discussion

A number of the properties of the sulfur and selenium compounds **4** are unique, and to this extent the materials defy classification. As a result we cannot give a complete picture of the underlying physics and chemistry entailed in the studies detailed above.

The one-dimensional structure is reminiscent of the charge-transfer compounds that constitute most of the synthetic conductors. The present materials differ in the absence of counterions in the lattice and in that the stacking is completely superimposed—most charge transfer salts adopt slipped stack arrangements. The structure shows the classic dimerization expected for a charge density wave in a half-filled band in a 1-d geometry. The fact that these are diradicals, however, leads to the unusual situation in which each molecule is connected to both of its nearest neighbors in the stack, with the 1,3-phenylene unit acting as a spacer. Although the central feature of the structure is the 1-d stacking, it is clear that three-dimensional interactions play an important role, particularly in the case of the selenium compound.

There are defect sites in the materials that are associated with paramagnetism and these are particularly obvious in the case of the sulfur compound. The easiest to visualize consists of a structure that appears to arise primarily by a dissociation of dimers to pairs of radicals that still undergo dipolar interaction. The defect that is present in greatest concentration in the sulfur compound appears to consist of an isolated spin-bearing dithiadiazolyl ring. This could be associated with a surface state or could arise from lattice defects. Nevertheless the orientation dependence of the solid-state ESR makes clear that the spin-bearing heterocyclic ring has the same orientation as its crystallographically ordered neighbors in the lattice. The fact that it seems to be this defect state that grows with increasing temperature shows that it can be formed directly from the crystallized material, as well as during the sublimation process.

The thermal defects do not appear to be associated with the conductivity in these materials—at least in the case of the sulfur compound. Nevertheless, these defects may be mobile. It seems fairly clear that the rapid relaxation seen in the NMR of these materials is best explained by mobile electrons. The presence of phase kinks would provide an explanation for the non-current-carrying mobile spins in the samples.

The model we propose for magnetic defects is shown in Chart I, where the heavy lines represent a side-on view of a 1-d stack of the individual molecules, the thin vertical lines connote radical–radical bonds at each end of the diradicals, and the solid dots represent unpaired spins. In structure A, the perfect diamagnetic lattice is shown, which gives way to the fragmented structure of B, in which there is an unpaired spin on the ends of two nearest neighbors in the lattice. This type of spin defect could be responsible for the dipolar coupling seen in the ESR spectrum of the sulfur compound, and a separation in the vicinity of 4 Å, between the radical sites, is consistent with the crystal structure, as this would leave about 3.5 Å between the spin-bearing rings and their other nearest neighbors in the stack. In C and D, one

Chart I

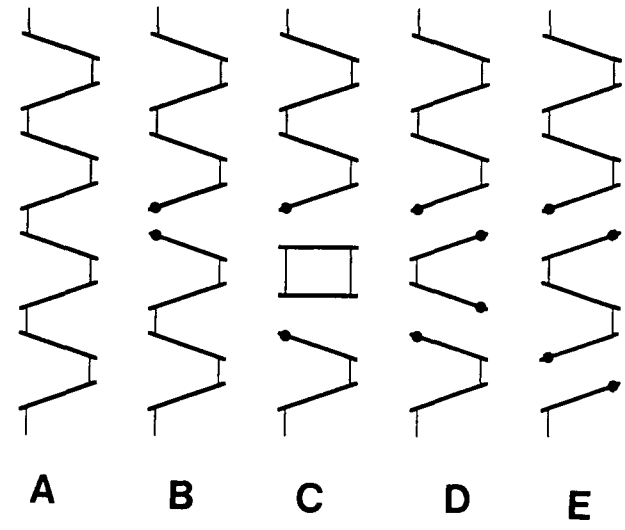

of the spins has begun to diffuse through the lattice. In C this is envisaged to occur by the formation of a simple cofacial dimer of the type seen in structure **3**,[9a] whereas D involves the creation of an additional pair of unpaired spins. In E the phase kinks that were introduced into the lattice in C and D have begun to separate. The phase kinks cannot annihilate by a simple dimerization, and they may have sufficient lifetime to propagate through the lattice and contribute to the magnetic and NMR behavior of the compounds. The activation energy derived from the ^{77}Se NMR relaxation times would therefore correspond to the energy required for the phase kinks to propagate through the lattice. In the model that we have advanced, thermal energy is implicated in (at least) two distinct processes: (i) the fragmentation of the radical–radical bonds and (ii) the reorientation of the molecules in the lattice as the spins diffuse (although these two processes could be coupled). The hysteresis seen in the magnetic susceptibility and ESR experiments on cooling samples that have been held at temperatures in the range 470–500 K would then be ascribed to phase kinks trapped in the lattice. The phase kink annihilation process would presumably require an activation energy for molecular reorientation that is comparable to that discussed above. The initial decrease in the concentration of spins in the sulfur compound just above room temperature suggests that, in this temperature regime, phase kink annihilation dominates the creation process (although this situation is soon reversed with increasing temperature).

Although we have implicated the diradical shown in B, as a structure such as this is suggested by the ESR spectra, it is possible that the dipolar coupling arises from a defect due to an absence in the lattice, as this would presumably be associated with two essentially unperturbed spin-bearing ring systems. If this is the case, the structure shown in B would be assigned a short lifetime in our model. Dipolar coupling due to the spin kink shown in D and E has not been seen in the ESR spectra.

While most of the foregoing discussion is concerned with the sulfur compound, these unusual paramagnetic effects are also thought to be operative in the selenium compound, although a high concentration of spins is never observed. In the model advanced above the paramagnetism is chiefly assigned to defects that disrupt the continuity of the lattice and do not provide carriers for conduction, although these spin excitations are probably responsible for the enhanced NMR relaxation times. This explanation would require that the charge carriers originate from thermal excitations between the valence and conduction bands, as in an intrinsic semiconductor.

Conclusion

We have now reported two groups of materials based on the neutral radical approach to conductors that utilize the 1,2,3,5-dithiadiazolyl and 1,2,3,5-diselenadiazolyl molecular building blocks. The structures of 1,4-phenylene bridged compounds

showed the presence of isolated dimers, although there was clear evidence of strong interactions between dimers.[9a] The structures of the 1,3-derivatives reported here are dominated by the 1-d stacking pattern and are clearly more akin to those of the molecular conductors based on charge-transfer salts. Nevertheless these materials also show a dimerization, together with strong interstack interactions. As a result of the dimerization there is an energy gap at the Fermi level in all of these materials and they are semiconductors. In order to stabilize highly conducting states in the neutral radical-based materials it will be necessary to overcome the charge density wave or Peierls distortion present in **3** and **4**. Just such a situation prevailed in the early charge-transfer conductors, and the remedies for this situation are well documented, although it should be noted that the half-filled band case (inherent in neutral radicals) is the energetically most favorable case for a charge density wave-driven structural instability and has never been suppressed in the case of the charge-transfer conductors. The dimensionality of the electronic structure is the key to stabilization of the metallic state, and this may be increased by the application of pressure and by the synthesis of compounds designed to foster anisotropic interactions. We are currently pursuing both of these directions.

Experimental Section

Starting Materials and General Procedures. 1,3-Dicyanobenzene, lithium bis(trimethylsilyl)amide, sulfur dichloride and selenium powder, and triphenylantimony were all obtained commercially (Aldrich). Sulfur dichloride was distilled before use and $LiN(SiMe_3)_2$ was converted into its diethyl etherate in order to facilitate amidine synthesis.[16] Acetonitrile (Fisher HPLC grade) was purified by distillation from P_2O_5. All reactions were performed under an atmosphere of nitrogen. Selenium tetrachloride[17] was prepared according to literature methods. Mass spectra were recorded on a Kratos MS890 mass spectrometer. ^1H NMR spectra were recorded at 400 MHz on a Bruker MH-400 spectrometer. Infrared spectra (CsI optics, nujol mulls) were obtained on a Nicolet 20SX/C FTIR instrument. Elemental analyses were performed by MHW laboratories, Phoenix, AZ. High-vacuum (pressures $\leq 10^{-6}$ Torr) sublimations were performed by using an Edwards ETP200 turbomolecular pump backed by an Edwards E2M8 two-stage mechanical pump.

Preparation of 1,3-[$(Me_3Si)_2N(Me_3SiN)CC_6H_4C(NSiMe_3)N(SiMe_3)_2$] (1,3-DIBADS). Solid $LiN(SiMe_3)_2{\cdot}Et_2O$ (49.3 g, 0.20 mol) was added to a slurry of 1,3-dicyanobenzene (13.1 g, 0.10 mmol) in 150 mL of diethyl ether, and the mixture was stirred at room temperature overnight. The majority of the solvent was then distilled off and replaced by 150 mL of toluene. A solution of Me_3SiCl (23.0 g, 0.20 mol) in 25 mL of toluene was then added, and the mixture was heated to gentle reflux for a further 24 h. The mixture was then cooled and filtered (to remove LiCl) and the solvent distilled from the filtrate to leave a dark brown oil. This oil was dissolved in 50 mL of hexane and the solution cooled to −30 °C to give (after several days) large crystalline blocks of 1,3-DIBADS (35.0 g, 0.58 mmol, 58%), mp 87 °C. ^1H NMR (δ, $CDCl_3$) 0.11 (s, 54 H, $SiMe_3$), 7.2–7.5 (m, 4 H, phenylene). Anal. Calcd for $C_{26}H_{58}N_4Si_6$: C, 52.46; H, 9.82; N, 9.41. Found: C, 52.21; H, 9.65; N, 9.43.

Preparation of 1,3-[$(S_2N_2C)C_6H_4(CN_2S_2)$]. A solution of SCl_2 (2.5 mL, 39 mmol) in 10 mL of CH_3CN was added to a slurry of 1,3-DIBADS (3.07 g, 5.15 mmol) in 100 mL of acetonitrile. The resulting mixture was heated at gentle reflux for 2 h and then filtered to afford crude 1,3-$[(S_2N_2C)C_6H_4(CN_2S_2)]^{2+}2Cl^-$ as an orange granular solid. This solid was then added to a solution of Ph_3Sb (2.14 g, 6.00 mmol) in 50 mL of acetonitrile, and the mixture was stirred rapidly and heated to about 60 °C for 2 h. The black precipitate was filtered off and dried in vacuo. The crude product (1.3 g), which is quite sensitive to oxygen, was then slowly (over several days) sublimed at 160–70 °C/10^{-2} Torr to afford small blue/black air-stable needles of 1,3-$[(S_2N_2C)C_6H_4(CN_2S_2)]$, mp 282–284 °C. The highest yield was 1.1 g (3.9 mmol, 78%), but yields were normally nearer 40%. IR (1600–250 cm^{-1}) 1357 (s), 1340 (s), 193 (m), 1163 (w), 1112 (w), 968 (m), 920 (w), 835 (w), 803 (m), 796 (m), 777 (s), 688 (s), 642 (s), 505 (s), 374 (m) cm^{-1}. Anal. Calcd for $C_8H_4N_4S_4$: C, 33.19, H, 1.42; N, 19.70; S, 45.09. Found: C, 33.62; H, 1.36; N, 19.50; S, 45.27. Mass spectrum (EI, 40 eV, m/e) 284 (M^+, 100%), 238 [$(M - SN)^+$, 25%], 206 [$(M - S_2N)^+$, 100%], 160 [$(SNCC_6H_4CN)^+$, 30%], 128 [$(NCC_6H_4CN)^+$, 100%], 78 (S_2N^+, 90%), 64 (S_2^+, 55%).

Preparation of 1,3-[$(Se_2N_2C)C_6H_4(CN_2Se_2)$]. A mixture of solid Ph_3Sb (7.05 g, 20.0 mmol) and 1,3-DIBADS (3.00 g, 5.0 mmol) was added through a powder funnel to a slurry of $SeCl_4$ (4.56 g, 20.5 mmol) in 125 mL of CH_3CN. This mixture was heated to reflux for 5 h, then cooled, and filtered to yield crude 1,3-$[(Se_2N_2C)C_6H_4(CN_2Se_2)]^{2+}2Cl^-$ as a dark brick red powder. This solid was then slurried together with a solution of Ph_3Sb (1.80 g, 5.1 mmol) in 100 mL of CH_3CN and the mixture heated to gentle reflux for 2 h. The black solid so produced was filtered, washed with 2 × 20 mL of CH_3CN, and dried in vacuo. The crude 1,3-$[(Se_2N_2C)C_6H_4(CN_2Se_2)]$ (2.05 g) was purified by sublimation at 180 °C/10^{-6} Torr to give fine golden needles, mp 302–304 °C. The highest yield of sublimed materials was 1.5 g (3.2 mmol, 61%), but yields were normally nearer 40%. IR (1600–250 cm^{-1}) 1342 (w), 1311 (w), 1286 (m), 1256 (w), 1151 (w), 916 (w), 797 (m), 736 (m), 720 (s), 690 (s), 639 (m), 615 (s), 395 (s) cm^{-1}. Anal. Calcd for $C_8H_4N_4Se_4$: C, 20.36; H, 0.85; N, 11.87. Found: C, 20.34; H, 1.01; N, 11.56. Mass spectrum (EI, 20 eV, m/e) 474 (multiplet, 17%, M^+), 398 [multiplet, 10%, $(M - Se)^+$], 302 [multiplet, 22%, $(M - Se_2N)^+$], 174 (multiplet, Se_2N^+, 30%), 160 (multiplet, Se_2^+, 100%), 128 [$(NCC_6H_4CN)^+$, 100%].

X-ray Measurements. All X-ray data were collected on an ENRAF-Nonius CAD-4 diffractometer at 293 K with monochromated Mo Kα (λ = 0.71073 Å radiation). Crystals were mounted on glass fibers with epoxy. Data were collected by using a $\theta/2\theta$ technique with a scan width of (1.0 + 0.3 tan θ). The selenium compound forms hairlike microcrystals; the small size of the crystals limited the number of data with $I > 2\sigma_I$ (less than 35% for $\theta\infty_{max}$ or 20°). The lack of high-angle data led to somewhat anomalous thermal parameters. Both structures were solved by using MULTAN and refined by full-matrix squares, which minimized $\sum w(\Delta F)^2$. Data collection, structure solution, and refinement parameters for both structures are available as supplementary material.

Conductivity Measurements. Conductivities as a function of pressure were measured in a Bridgman anvil cell using isomica washers to contain the sample. The resistance between the pole faces was used to calculate the conductivity after correction for the sample geometry. Pressure was applied with a hydraulic press of 50-ton capacity. The cell was calibrated with a standard bismuth sample according to literature results.[18] The single-crystal measurements were made along the long (c) axes of the crystals, using silver–epoxy to attach the leads to the samples. In order to obtain electrical contact with the selenium compound, gold pads were first evaporated onto the sample. Four-point measurements were made in an argon atmosphere, using a Keithley 236 with a constant voltage drop of 10 V over the voltage leads.

Magnetic Susceptibility Measurements. The magnetic susceptibility was measured from 4.2 to about 650 K by using the Faraday technique. Details of this apparatus have been previously described.[19] The applied field was 1.4 T and the measured susceptibility was checked for field dependence at several temperatures.

ESR Spectra. Solution-based ESR spectra were recorded by using a Varian E-109 spectrometer on samples dissolved in chloroform (predried over P_2O_5); samples were degassed by a series of at least five freeze/pump/thaw cycles. The solid-state ESR measurements were made on a custom-built computer-controlled instrument, using a Varian 1-T magnet. Crystals were contained in 1-mm quartz capillaries terminated in a narrow slot to maintain their orientation.

Solid-State NMR Measurements. ^1H spectra and relaxation rates were obtained on Chemagnetics CMX and Bruker MSL spectrometers, operating at fields of 2.35 and 7.05 T, respectively. ^{77}Se spectra and relaxation rates were measured on Bruker MSL and CXP spectrometers, at fields of 7.05 and 4.70 T, respectively. Spin–lattice relaxation rates were obtained in saturation–recovery (^1H) and inversion–recovery (^{77}Se) experiments. MAS spectra were recorded at a spinning frequency of 6.15 kHz, using a Doty Scientific MAS probe. The static and MAS spectra in Figure 12 are the results of 180 000 and 144 000 scans, respectively. The static spectrum was obtained in a spin echo experiment, with a pulse spacing of 60 μs.

Band Structure Calculations. The band structures were carried out with the EHMACC suite of programs using parameters discussed previously.[9a,20,21] The off-diagonal elements of the Hamiltonian matrix were calculated with the standard weighting formula.[22]

(16) Boeré, R. T.; Oakley, R. T.; Reed, R. W. *J. Organomet. Chem.* **1987**, *331*, 161.

(17) Brauer, G. *Handbook of Preparative Chemistry*; Academic: New York, 1963; Vol. 1, p 423.

(18) Andersson, G.; Sundqvist, B.; Bäckström, G. *J. Appl. Phys.* **1989**, *65*, 3943.

(19) (a) DiSalvo, F. J.; Waszczak, J. V. *Phys. Rev.* **1981**, *B23*, 457. (b) DiSalvo, F. J.; Menth, A.; Waszczak, J. V.; Tauc, J. *Phys. Rev.* **1972**, *B6*, 4574.

(20) See ref 6a for a discussion of the Hückel parameterization of SN rings.

(21) Basch, H.; Viste, A.; Gray, H. B. *Theor. Chim. Acta* **1965**, *3*, 458.

Acknowledgment. Financial support at Guelph was provided by the Natural Sciences and Engineering Research Council of Canada and at Arkansas by the National Science Foundation (EPSCOR program) and the State of Arkansas. R.C.H. wishes to acknowledge valuable discussions with D. W. Murphy, B. Golding, P. B. Littlewood, A. P. Ramirez, and W. W. Warren.

(22) Ammeter, J. H.; Burghi, H. B.; Thibeault, J. C.; Hoffman, R. *J. Am. Chem. Soc.* **1978**, *100*, 3686.

Supplementary Material Available: Tables of crystal data, structure solution and refinement (S1), atom coordinates (S2), bond lengths and angles (S3), and anisotropic thermal parameters (S4) for both structures 1,3-[$(E_2N_2C)C_6H_4(CN_2E_2)$] (E = S, Se) (10 pages). Ordering information is given on any current masthead page.

Local Effect of Glycine Substitution in a Model Helical Peptide

Pingchiang C. Lyu, Ping Chuan Wang, Mark I. Liff, and Neville R. Kallenbach*

Contribution from the Department of Chemistry, New York University, New York, New York 10003. *Received July 24, 1990*

Abstract: The amino acid glycine strongly destabilizes α-helical structure in proteins as well as in model helical peptides. We have investigated the role of a single glycine substitution in a helical host peptide system. Quantitatively, a single glycine → leucine substitution has about one-third of the effect on the stability of helix as does triple substitution of these residues in the middle of the helix. The single glycine perturbs the distribution of helix in the peptide. NMR experiments detect a strong local drop in helix structure at the residues flanking the site of substitution, in addition to overall loss in helicity of the peptide seen at all positions in the chain.

Introduction

The α-helix[1] is the single most abundant secondary structure in globular proteins.[2] The factors that stabilize α-helical structure are of fundamental importance in understanding how structure is acquired,[3] both in isolated fragments of proteins and in intact protein chains. In some, but not all,[4] cases α-helices serve as early intermediates in the folding of globular proteins. Polypeptides of different composition[3] and peptides of different sequence[5-10] exhibit varying degrees of helicity, so that each side chain in a helix appears to influence the helical structure present. Alanine and leucine are well-known to stabilize α-helical structure, for example, whereas proline and glycine destabilize helices.[9,10] But how or why a particular side chain influences the stability of α-helix is not clear; it seems likely that no single mechanism will account for the role of all side chains. The intrinsic strength of hydrogen bonds in the helix must depend on the nature of the donor and acceptor side chains. Inspection of helix wheels[11] shows that longer range interactions among side chains along the helix are possible, particularly if the spacing of groups is appropriate. Thus charges or nonpolar side chains spaced at intervals of i, $i + 4$ lie on the same face of the helix and can presumably influence each other. On the other hand differences among chemically similar side chains such as leucine, isoleucine, and valine[6c,7c,9,10] in identical environments imply that there are short-range effects of single substitution as well. The conformational restriction imposed by α-helix formation has been shown to be a significant factor in the helix propensities of chemically similar side chains.[12]

We have investigated[10] a series of peptides that we refer to by the standard one-letter abbreviations for the three "guest" amino acids which are introduced into the central positions in "host" chains with the sequence

succinyl-Tyr-Ser-Glu_4-Lys_4-XXX-Glu_4-Lys_4-NH_2

CD spectroscopy of ten substituted chains allows us to assign an order of relative helix stabilizing effect to the different guest amino acids in the series:[10] Ala > Leu > Met > Gln > Ile > Val > Ser > Thr > Asn > Gly. This order is consistent with that determined in a series of host-guest coiled-coil peptides by O'Neil and DeGrado,[9] but not with host-guest experiments on polyamino acids with alkylated glutamic acid as host side chains.[5] NMR analysis of members of the series indicates that each is partially helical, with the helix favoring the N terminus of the chain.[13] This analysis is based on distance criteria and coupling constants and shows that the chemical shift of the Cα protons in the host blocks of these peptides affords a useful measure of the helix probability.

The question that concerns us here is how a single substitution stabilizes α-helix relative to the triple substitutions used previously

(1) Pauling, L.; Corey, R. B.; Branson, H. R. *Proc. Natl. Acad. Sci. U.S.A.* **1951**, *37*, 205.
(2) Creighton, T. E. *Proteins*; W. H. Freeman: New York, 1984.
(3) Sueki, M.; Lee, S.; Powers, S. P.; Denton, J. B.; Konishi, Y.; Scheraga, H. A. *Macromolecules* **1984**, *17*, 148.
(4) (a) Roder, H.; Elove, G. A.; Englander, S. W. *Nature* **1988**, *335*, 700. (b) Udgaonkar, J. B.; Baldwin, R. L. *Nature* **1988**, *335*, 694.
(5) (a) Brown, J. E.; Klee, W. A. *Biochemistry* **1971**, *10*, 470. (b) Bierzynski, A.; Kim, P. S.; Baldwin, R. L. *Proc. Natl. Acad. Sci. U.S.A.* **1982**, *79*, 2470. (c) Kim, P. S.; Bierzynski, A.; Baldwin, R. L. *J. Mol. Biol.* **1982**, *162*, 187. (d) Shoemaker, K. R.; Kim. P. S.; Brems, D. N.; Marqusee, S.; York, E. J.; Chaiken, I. M.; Stewart, J. M.; Baldwin, R. L. *Proc. Natl. Acad. Sci. U.S.A.* **1985**, *82*, 2549. (e) Shoemaker, K. R.; Kim, P. S.; York, E. J.; Stewart, J. M.; Baldwin, R. L. *Nature* **1987**, *326*, 563. (f) Strehlow, K. G.; Baldwin, R. L. *Biochemistry* **1989**, *28*, 2130. (g) Shoemaker, K. R.; Fairman, R.; Schultz, D. A.; Robertson, A.; York, E. J.; Stewart, J. M.; Baldwin, R. L. *Biopolymers* **1990**, *29*, 1.
(6) (a) Marqusee, S.; Baldwin, R. L. *Proc. Natl. Acad. Sci. U.S.A.* **1987**, *84*, 8988. (b) Marqusee, S.; Robbins, V.; Baldwin, R. L. *Proc. Natl. Acad. Sci. U.S.A.* **1987**, *86*, 5286. (c) Padmanabhan, S.; Marqusee, S.; Ridgeway, T.; Lane, T. M.; Baldwin, R. L. *Nature* **1990**, *344*, 268.
(7) (a) Merutka, G.; Stellwagen, E. *Biochemistry* **1989**, *28*, 352. (b) Merutka, G.; Stellwagen, E. *Biochemistry* **1990**, *29*, 894. (c) Merutka, G.; Lipton, W.; Shalongo, W.; Park, S.-H.; Stellwagen, E. *Biochemistry* **1990**, *29*, 7511.
(8) (a) Lyu, P. C.; Marky, L. A.; Kallenbach, N. R. *J. Am. Chem. Soc.* **1989**, *111*, 2733. (b) Lyu, P. C.; Marky, L. A.; Kallenbach, N. R. *Peptides, Proceedings of the Eleventh American Peptide Symposium*; Rivier, J. E., Marshall, G. R., Eds.; ESCOM: Leiden, 1990; p 632.
(9) O'Neil, K. T.; DeGrado, W. F. *Science* **1990**, *250*, 646.
(10) Lyu, P. C.; Liff, M. I.; Marky, L. A.; Kallenbach, N. R. *Science* **1990**, *250*, 669.
(11) Schiffer, M.; Edmundsen, A. B. *Biophys. J.* **1967**, *7*, 121.
(12) (a) Hermans, J.; Yun, R.-H.; Anderson, A. G. Private communication. (b) Piela, L.; Nemethy, G.; Scheraga, H. A. *Biopolymers* **1987**, *26*, 1273.
(13) Liff, M. I.; Lyu, P. C.; Kallenbach, N. R. *J. Am. Chem. Soc.* **1991**, *113*, 1014.

0002-7863/91/1513-3568$02.50/0